J Fluoresc (2012) 22:281–288
DOI 10.1007/s10895-011-0958-4

ORIGINAL PAPER

Detection and Evaluation of Normal and Malignant Cells Using Laser-Induced Fluorescence Spectroscopy

Mohamad E. Khosroshahi · Mahya Rahmani

Received: 29 June 2011 / Accepted: 30 August 2011 / Published online: 8 September 2011

Abstract The aim of this research is to study the normalized fluorescence spectra (intensity variations and area under the fluorescence signal), relative quantum yield, extinction coefficient and intracellular properties of normal and malignant human bone cells. Using Laser-Induced Fluorescence Spectroscopy (LIFS) upon excitation of 405 nm, the comparison of emission spectra of bone cells revealed that fluorescence intensity and the area under the spectra of malignant bone cells was less than that of normal. In addition, the area ratio and shape factor were changed. We obtained two emission bands in spectra of normal cells centered at about 486 and 575 nm and for malignant cells about 482 and 586 nm respectively, which are most likely attributed to NADH and riboflavins. Using fluorescein sodium emission spectrum, the relative quantum yield of bone cells is numerically determined.

Keyword Fluorescence spectroscopy · Laser · Quantum yield · Area ratio · Cell discrimination

Introduction

Osteosarcoma represents the most common sarcoma of bone, accounting for about one-quarter of all primary malignancies of bone and about one-third of all bone sarcomas. The incidence rates and 95% confidence intervals of osteosarcoma for all races and both sexes are 4.0 (3.5–4.6) for the range 0–14 years and 5.0 (4.6–5.6) for the range 0–19 years per year per million persons. Among childhood cancers, osteosarcoma generally occurs in 2.4% of all malignant tumor cases. The incidence rates of childhood and adolescent osteosarcoma in Blacks and Hispanics is more than Caucasian and it has always been considered to be higher in males than in females, occurring at a rate of 5.4 per million persons per year in males vs. 4.0 per million in females. Osteosarcoma has a bimodal age distribution, having the first peak during adolescence (10–14-year-old age group) and the second peak in older adulthood (in adults older than 60 years old) [1–3].

Bone marrow metastases are detected by Imaging such as skeletal scintigraphy [4], radiography [5], computed tomography [6], or magnetic resonance imaging (MRI) [7] and the other methods such as positron emission tomography or single-photon emission computed tomography have a potential of evaluating it [8].When luciferase(Lus) or the green fluorescent protein (GFP) transfected cells are used, whole-body bioluminescent reporter imaging (BRI) [9, 10] can detect microscopic bone marrow metastases, too. Polymerase chain reaction-based (PCR) methods with serious limitations [11] and immunocytochemical techniques [12] are the other useful detection and quantification of cancerous bone marrow cells.

In recent years, many optical methods are applied for biological and biomedical investigations. Light-induced fluorescence spectroscopy (LIFS) is one of the most widely spread spectroscopic methods which finds biomedical applications especially in diagnosis of cancer [13–16]. Fluorescence is the emission of light typically from aromatic molecules and depending on the nature of the excited state. In singlet excited states, the electron in excited orbital is paired (by opposite spin) to the second electron in the ground-state orbital. Consequently, return to the ground state is spin allowed and occurs rapidly by

M. E. Khosroshahi (✉) · M. Rahmani
Faculty of Biomedical Eng., Biomaterial Group,
Laser and Nanobiophotonics Lab,
Amirkabir University of Technology,
Tehran, Iran
e-mail: khosro@aut.ac.ir

emission of a photon [17]. This technique has been applied for the in vitro and in vivo analysis. In LIFS low-power laser light is directed toward biological component (such as biologic fluids, single cells, cell suspensions, frozen tissue sections and bulk tissues), inducing fluorescence emission at wavelengths characteristic of the chemical composition of the biomaterials. The excitation light used for fluorescence measurements is usually in the near-UV and visible region. The advantages of using LIFS diagnosis are that the measurements are safe and noninvasive and can be performed quantitatively and quickly [18, 19].

The fluorescence technique can be automated and offers real-time detection and differentiation with a precision, selectivity and sensitivity. In general, the predictive accuracy of spectroscopy is better than prediction based on biopsy solely. In contrast to conventional biopsy techniques, light and laser-induced fluorescence spectroscopy can be conducted to characterize tissues or to detect cancers without removing them [20–22]. If fluorescence could be used as a complementary method; then it could be of great interest in many clinical specialties. This would hopefully reduce the sampling error and help avoid unnecessary biopsies. Fluorescence spectroscopy also introduces other advantages such as short pulse excitation, wavelength tunability, and narrow bandwidth excitation [19]. By using different excitation wavelengths and spectral analysis techniques, fluorescence spectroscopy was subsequently used for distinguishing premalignant, malignant and normal tissues in a variety of organ systems, such as lung and breast [13, 23], bronchus [24], colon [25, 26], cervix [27], esophagus [28], and head and neck [29].These alternations that occur as tissue progresses from a normal to a diseased state are reflected in the spectral characteristics of the measured fluorescence. The endogenous fluorophores such as the reduced form of nicotinamide adenine dinucleotide (phosphate) (NA(P)DH) and riboflavins (flavin mononucleotide (FMN) and flavin adenine dinucleotide (FAD)), collagen, elastin, amino acids, vitamins, lipids and porphyrins have a significant variation in the concentration in different tissue types. These differences, together with alternations in the local environment within the tissue, are the basis for the discrimination between tumor and normal tissue by fluorescence spectroscopy. Characterizing biological samples such as cells or tissues can be performed by steady-state fluorescence measurements in terms of overall intensity, peak wavelength and spectral shape [17, 18, 30].

The complicated analysis of tissues spectra due to strong light scattering because of structural heterogeneity and the need for improved sensitivity and specificity in cancer diagnosis has led to interest in native cellular fluorescence instead of frozen tissue section or bulk tissue fluorescence [31].

In diagnostic method for cancer detection it is essential to separate malignant tumors from normal tissues. The goal of this study was to use LIFS to discriminate normal and malignant human bone cells and systematically characterize the differences in fluorescence properties such as area ratio, shape factor, extinction coefficient and quantum yield on emission spectra upon excitation at 405 nm.

Materials and Method

Preparation of Cell Suspensions Human osteosarcoma cell line (G 292, NCBI-C565) which was initiated from a primary bone tumor osteosarcoma, purchased from national cell bank of Pasteur institute of Iran. Normal osteoblast cell (HOB) were extracted by MACS (Magnetic activated cell sorting) method and measurements were made on cells having passage numbers of 30 or less. The G 292 cells were grown in Dulbecco modified Eagle medium (DMEM, GIBCO 116–12800) supplemented with 10% fetal bovine serum (FBS, GIBCO 106–10270). The HOB cells were grown in DMEM and HAM'S F12 (Sigma-Aldrich N6658) in ratio of 1:1, supplemented with 12% FBS. Both cells supplemented with 1% Antibiotic-Antimycotic Solution (PAA, P11-002) and then cells were incubated at 37 °C with 5% CO_2. Upon reaching confluence for G 292 cells and pre-confluence for HOB cells, (generally 3 days after passage), these cells were collected from culture flasks by trypsinization to yield a suspension and washed with phosphate-buffered saline (PBS) (GIBCO 18912–014). After washing, the cells were resuspended in a volume of 2 mL PBS. The cell suspensions pipetted into a cuvette with 1 cm path length for LIFS analysis. Cell concentration was determined by counting the number of cells per milliliter (cells/mL) manually in a standard manner with a haemocytometer from Neubauer and light microscope. The average cell viability determined with a manual viability count after addition of Trypan Blue 0.25% in PBS. The measurements were repeated independently three times for each sample.

Fluorescence Spectroscopy of Cell Suspensions A schematic diagram of the LIFS configuration is shown in Fig. 1 As it is shown in Fig. 1, a laser with 405 nm wavelength (CSI-405) with 100 mW maximum output power was used as an excitation source. An optical fibre with 600 μm core diameter and 0.22 NA (Ocean Optic .LIBS-600-6-SR) was used to collect the fluorescence signal and guide it to the spectrometer (Ocean Optic, UV–VIS USB2000). The background spectrum was first recorded from cuvette filled with PBS solution and then the fluorescence measurements of cell suspensions were made at room temperature. After obtaining the spectra of samples, they were smoothened by Gaussian

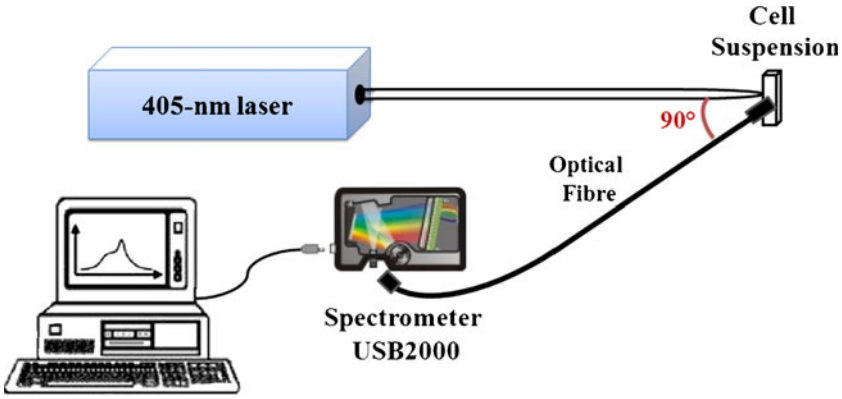

Fig. 1 Schematical diagram of the LIFS experimental set-up with excitation at 405 nm

model using FindGraph software. In order to determine the relative quantum yield, 10^{-2} mM fluorescein sodium solution was used as a reference solution. After solving fluorescein sodium powder (Merck, 518-47-8) in distilled water with stirring and then filtration, the measurement was occurred.

Results

The spectrum of the excitation light source is shown in Fig. 2. The average cell viability was 89.3±3.8% and cell concentration for normal HOB and malignant G 292 were 9.4×10^5 and 8.6×10^5 cell/lit, respectively.

The 405 nm laser induced-fluorescence spectra of normal HOB and malignant G 292 cell which is normalized to the HOB fluorescence peak at 486 nm (peak intensity of normal cell), are shown in Fig. 3. It can be seen that after samples excitation two peaks are observed at 486 and 575 nm corresponding to HOB cells, while that of malignant G 292 cells are slightly shifted to 482 and 586 nm, respectively. A considerable decrease in fluorescence amplitude of malignant G 292 cells compared to normal HOB cells can be seen and the main difference is observed in the region of 470–590 nm. This decrease can be explained in terms of biochemical and microstructural changes due to abnormalities. Main broad emission in the region of 470–490 nm were attributed to NADH [32–35] and Secondary broad emission in the region of 570–590 nm is most likely attributed to riboflavins [36, 37].

The comparison of laser induced-fluorescence spectra normalized to the main peak is presented in Fig. 4. When the peak intensities of the normal and malignant spectra are normalized, the differences in spectral line shape become more evident. The spectral line shapes of normal HOB and malignant G 292 cells are slightly different in the region of 530–610 nm.

In order to develop an algorithm for disease classification based on the spectral differences, the ratio between two fluorescence peaks in each spectrum as shape factor, R_1 ratio, must be considered. The peak fluorescence intensities and R_1 ratio is shown in Table 1. Also, R′ parameter which is defined as intensity ratio of normal HOB over malignant G 292 cell, is shown in the Table 2. A decrease of fluorescence intensities of malignant G 292 comparing with normal HOB is noticeable and being is stronger at about 484 nm.

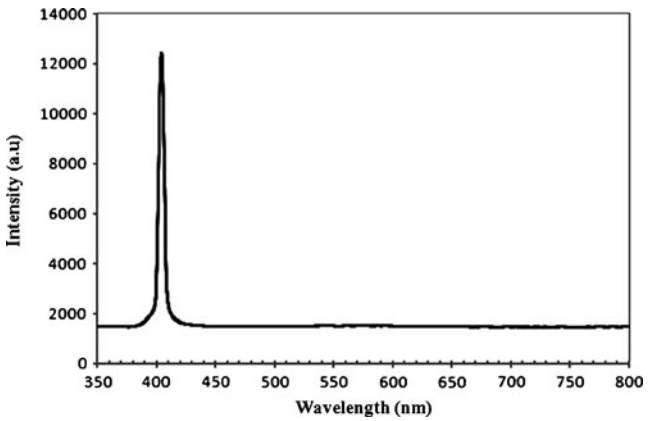

Fig. 2 405 nm laser beam spectrum

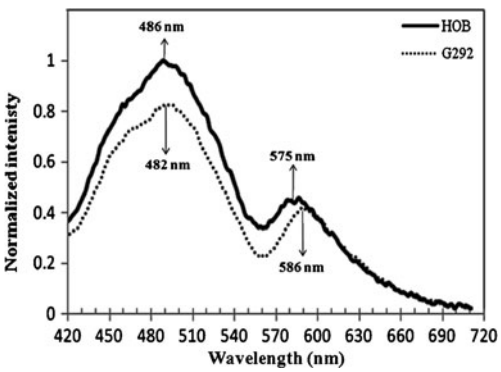

Fig. 3 Fluorescence emission spectra of normal HOB and malignant G 292 cells. Malignant G 292 cell is normalized to the HOB fluorescence peak at 486 nm by FindGraph

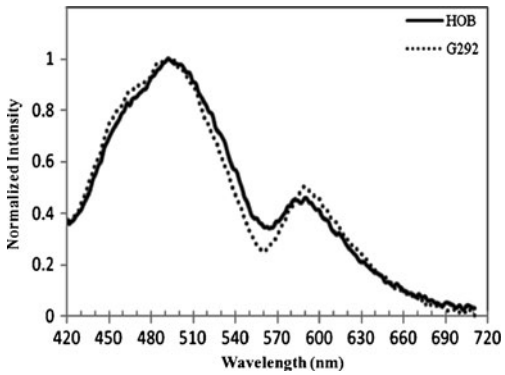

Fig. 4 Fluorescence emission spectra of normal HOB and malignant G 292 cells normalized to main peak by FindGraph

To intensify spectral structure differences of the fluorescence signal, each fluorescence spectrum was evaluated by area under the normalized fluorescence peak signal and area ratio (R_S). It turned possible to notice slight differences among the spectra and identify parameters with the best distinction. It is visually obvious in Fig. 3 that the spectrum of G 292 malignant sample have smaller area than the HOB normal. Although, these differences aren't always visually obvious, the area under the fluorescence peak signals and also R_s parameter is calculated by FindGraph software and it is shown in Table. 3. Based on normalized area measurement, the decrease of area under the fluorescence peak of malignant G 292 cell comparing with normal HOB cell is significant. Moreover, Rs parameter can be calculated by using ($R_S = \frac{S_{HOB}}{S_{G\,292}}$). Note that R_S is 1.25 (R_S>1), thus, the discrimination is numerically meaningful.

Relative Quantum Yield

Theory Considering that there are three processes of returning to ground state ie. radiationless energy loss, intersystem crossing via triplet state and emission of photon, then the efficiency of emission which is defined as Eq. 1 will be a function of the competiting rates of these processes:

$$q = \frac{k_f}{k_f + k_i + k_x} \tag{1}$$

Table 1 Fluorescence intensities at ~484 and ~580 nm and intensity ratio (R_1) for malignant and normal cells

	I_{max} (~484)	I_{max} (~580)	$R_1=I_{484}/I_{580}$
G292	0.80	0.44	1.82
HOB	0.98	0.45	2.18

Table 2 Intensity ratio (R′) of normal HOB over malignant G 292 cell samples

	λ=484 nm	λ=580 nm
$R'=I_{HOB}/I_{G292}$	1.23	1.02

Where q is the efficiency of emission or quantum yield and k_f is the rate constant for fluorescence emission, k_i the rate constant for radiationless energy loss, and k_x the rate constant for intersystem crossing. The term k_f also relates to the average life time of the excited state τ_a by the equation $k_f=\tau_a^{-1}$. The average life time is used since any one molecule can emit light at many probable times, smaller or greater than τ_a. However because of some problems associated with absolute quantum yield measurements such as complicated calculations and instrumentation, several simple relative methods have been devised which substitute a compound of "known" quantum yield in place of a standard scattered as a reference. This method consists simply of comparing the fluorescence intensity of sample under study to the intensity of a dye of known quantum yield. For the calculation of relative quantum yield, the Eq. 2 was used:

$$\frac{F_X}{F_S} = \frac{Q_X I_{EX} \%A_X G(\theta)_X}{Q_S I_{ES} \%A_S G(\theta)_S} \tag{2}$$

Where F_X is the measured fluorescence of unknown and F_S is that of the standard dye solution, Q_X and Q_S is the quantum yield of known and the standard dye solution, I_{EX} and I_{ES} is the intensity of exciting light of known and the standard dye solution, $\%A_S$ and $\%A_X$ is the percent absorption of solution (100-T%),$G(\theta)_S$ and $G(\theta)_X$ is geometry factor of standard dye solution and measured fluorescence of known (<1 since not all of the fluorescent light observed),respectively. By exciting both samples at the same wavelength, having the solutions of equal absorbency at this wavelength and using the same set-up, the value of Eq. 3 will also be unity:

$$\frac{I_{EX} \%A_X G(\theta)_X}{I_{ES} \%A_S G(\theta)_S} = 1 \tag{3}$$

Table 3 The area under the peak of normalized fluorescence signals and area ratio

	$S = \int_{x_1}^{x_2} y\,dx, (x_1 = 420, x_2 = 650)$
G 292	104.13
HOB	129.95

Consequently, the ratio of the quantum yield of standard and unknown sample is:

$$\frac{F_X}{F_S} = \frac{Q_X}{Q_S} \tag{4}$$

To estimate the quantum yields for compounds emitting below 600 nm, Eq. 4 is suitable and practical. If a spectrometer system is used instead of monochromator-photomultiplier, one must integrate the total area under emission spectrum for both unknown and standard sample and use the area ratio ($\frac{S_X}{S_s}$) in preference to intensity ratio in Eq. 4 [38, 39]. Among many possible dyes to choose as a reference standard for quantum yield determination, we choose 10^{-2} mM fluorescein sodium solution with 0.79± 0.06 reported quantum yield [39]. Its emission spectrum in arbitery unit is shown in Fig. 5 The area under the peak of reference solution in the region of 500–650 nm which was calculated by FindGraph software, is 46487.6. By considering the main fluorescence peak of cell samples, the area under the fluorescence peak in arbitery unit was calculated. Table 4 shows the quantum yield calculations of normal HOB and malignant G 292 cells using Eq. 4.

Extinction Coefficient Calculation A fundamental aspect of fluorescence spectroscopy is the evaluation of light absorption and extinction coefficient. The Lambert–Beer low is used to measure the absorption experimentally, and is expressed by Eq. 5:

$$log\frac{I_0}{I} = \epsilon cd \tag{5}$$

Where I_0 and I are the light intensities as the light enters and leaves the absorbing medium, ε is the molar extinction coefficient in M^{-1} cm^{-1}, c is the concentration in mol/L (M) and d is the path length in cm. Assuming 10% light absorption by cell suspension (I_A=0.1I_0) occurred and c≅9.0×10^5 cell/mL, ϵ is calculated by Beer–Lambert low:

$$log\frac{I_0}{0.9\,I_0} = \epsilon \times 9.0 \times 10^5 \times 10^{-3} \times 1 \rightarrow \epsilon \cong 5 \times 10^{-5} \quad (cm^2.cell^{-1})$$

Discussion

In this study, we observed a significant difference between the fluorescence spectra of normal and malignant cell samples. This is due to differences in intrinsic fluorescence properties of normal and malignant cells reflecting the amount of different present fluorophores and the properties of surrounding microenvironment. Previous studies on fluorescence-Excitation Emission Matrix (EEM) of different cells revealed the role of three principal endogenous fluorophores in cellular fluorescence. Depending on the excitation wavelength, it is provided by tryptophan, NAD(P)H and riboflavins (FMN, FAD). NADH and riboflavins which correlate specifically with cellular activity can provide information about the metabolic changes within cells [36, 40–42]. In fact, we found the NADH and riboflavins fluorescence spectra decreased with malignancy and it is due to deficiency of aerobic oxidation system. In other words, when malignant cells proliferate quickly, the ratio between the oxidized (NAD^+) and reduced form (NADH) of NAD alters and the accumulation of less fluorescent NAD^+ results in the decreased fluorescence in cancer [33, 43–46].

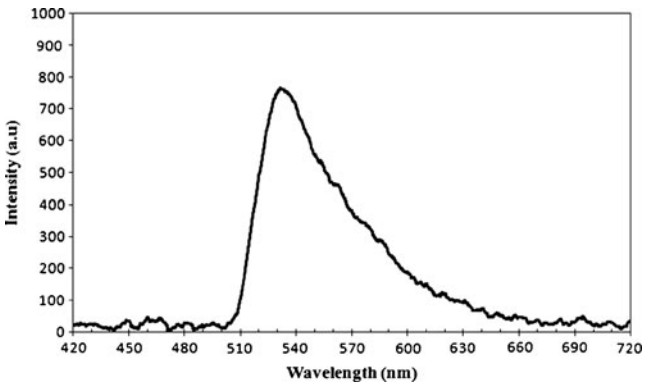

Fig. 5 The spectrum of Fluorescein sodium solution used as a standard reference and excited by 405 nm

It seems the observed blue and red shifts of NADH and riboflavins band from normal to malignant cells to be due to the physiological and biochemical transformation of normal into cancerous cells. Membrane potential abnormalities, mineral cell content and membrane composition changes are due to changes in the dielectric properties of normal cells during its transformation to a cancer cell [23,

Table 4 The quantum yield calculation of normal HOB and malignant G 292 cells using Eq. 4. The area under the main peak of reference solution and cell samples calculated by FindGraph

Cell sample	$S_{(435–545\ nm)}$	$Q_X = \frac{S_X Q_S}{S_s}$	% Q
Malignant G 292	1709.16	$Q_{G292} = \frac{1709.16\times0.79}{46487.6} = 0.029$	2.9%
Normal HOB	1962.91	$Q_{HOB} = \frac{1962.91\times0.79}{46487.6} = 0.033$	3.3%

47, 48].However, the influence of multiple light elastic scattering of cells arising from Rayleigh scattering on the wavelengths shifts has to be considered [46] Based on normalized intensity evaluation, the fluorescence peak decrease would allow clear discrimination between normal and malignant cells. To overcome the limitations of numerical intensity measurements, the use of a dimensionless ratio $R_1=I_{484}/I_{580}$ as a shape factor is preferred. The fact that both intensities are equally influenced by experimental parameters indicates the very distinct shapes of normal and malignant spectra. A major advantage of this ratio is that the difference in intensity ratio at these two wavelengths can be attributed to the difference in the fluorescence yield of the native fluorophores (i.e., NAD(P)H, riboflavins) for various cell types. Ratio R_1 was found to have a definite diagnostic potential in different kinds of cancer [27, 36, 49–52].

The shape distortion of the fluorescence spectra due to absorption of native fluorophores could lead to appearance of false maxima [53]. In order to avoid this misunderstanding, normalized fluorescence spectra of both cells were evaluated. It's obvious that the spectral line shape of normal and malignant cell samples are slightly different. In addition to intensity changes, it can be seen that the spectral shape of normal and malignant bone cells alters by increasing ratio R_1. The R′ value is found to be maximal at about 484 nm NADH emission with greatest spectral discrepancy. Thus, this wavelength should be convenient to maximize cancer discrimination.

R. Hage et al. [54], Wei Chen et al. [55]. believe that one of the most accurate parameters that showed the best performance in the discrimination of different samples were the area under the peak of fluorescence signals We expect that the area under the fluorescence peak of normal cell should be larger than the malignant one due to the intense metabolic activity of the malignant tumor cell and our experimental fluorescence spectra indicated a significant decrease with malignancy. Finally, in our case, R_S = 1.25 ($R_S>1$) which is a suggestive ratio for indicating the discrimination between normal and malignant bone cells.

Conclusion

In this research the LIFS technique demonstrated its ability to discriminate between normal and malignant bone cells due to intracellular fluorophores mainly NADH and riboflavins which presented the metabolic activity of cells. By normalized intensity, a significant decrease in fluorescence spectra with malignancy was observed. In addition to intensity variations, it was seen that the ratio R_1 increases due to changes in spectral shape of both normal and malignant cells. This shows that the contribution of NADH relative to riboflavins in creating normal cell spectra is more than malignant one. Due to the physiological and biochemical transformation of normal cells, 4 nm spectral blue shift and 9 nm spectral red shift which are observed due to NADH and riboflavins bands. Moreover, Intensity ratio ($R'=1.23$) is found to be maximal at about 484 nm and it confirms NADH emission band carries greatest spectral discrimination. Therefore, this wavelength should be convenient to maximize the ability of cancer discrimination. Experimental fluorescence spectra indicated significant decrease in area under the fluorescence spectrum with malignancy and R_S ($R_S=1.25$, $R_S>1$) is a suggestive ratio for indicating the discrimination between normal and malignant bone cells. We calculated the relative quantum yield of bone cells at about 3% and extinction coefficient of about 5×10^{-5} $cell^{-1}$ cm^2.

Acknowledgements We would like to acknowledge Dr MA Shokrgozar and Dr N.Haghighipour from national cell bank of Pasteur institute of Iran and Dr E. Mohajerani from laser research institute of Shahid Beheshti university.

References

1. Alison MR (2004) The cancer handbook. Wiley, United State
2. Ottaviani G, Jaffe N (2010) The epidemiology of osteosarcoma. Cancer Treat Res 152:3–13
3. Mirabello L, Troisi RJ, Savage SA (2009) Osteosarcoma incidence and survival rates from 1973 to 2004. Cancer 115:1531–1543
4. Even-Sapir E (2005) Imaging of malignant bone involvement by morphologic, scintigraphic, and hybrid modalities. J Nucl Med 46 (8):1356–1367
5. Rybak LD, Rosenthal DI (2001) Radiological imaging for the diagnosis of bone metastases. Q J Nucl Med 45(1):53–64
6. Fogelman I, Cook G, Israel O, Van der Wall H (2005) Positron emission tomography and bone metastases. Semin Nucl Med 35 (2):135–142
7. Mentzel HJ, Kentouche K, Sauner D, Fleischmann C, Vogt S, Gottschild D, Zintl F, Kaiser WA (2004) Comparison of whole-body STIR-MRI and 99mTc-methylene-diphosphonate scintigraphy in children with suspected multifocal bone lesions. Eur Radiol 14(12):2297–2302
8. Hamaoka T, Madewell JE, Podoloff DA, Hortobagyi GN, Ueno NT (2004) Bone imaging in metastatic breast cancer. J Clin Oncol 22(14):2942–2953
9. Yang M, Baranov E, Jiang P, Sun FX, Li XM, Li L, Hasegawa S, Bouvet M, Al-Tuwaijri M, Chishima T, Shimada H, Moossa AR, Sheldon P, Hoffman RM (2000) Whole-body optical imaging of green fluorescent protein-expressing tumors and metastases. Proc Natl Acad Sci USA 97(3):1206–1211
10. Wetterwald A, van der Pluijm G, Que I, Sijmons B, Buijs J, Karperien M, Löwik CW, Gautschi E, Thalmann GN, Cecchini MG (2002) Optical imaging of cancer metastasis to bone marrow: a mouse model of minimal residual disease. Am J Pathol 160(3):1143–1153
11. Zippelius A, Kufer P, Honold G, Köllermann MW, Oberneder R, Schlimok G, Riethmüller G, Pantel K (1997) Limitations of reverse-transcriptase polymerase chain reaction analyses for detection of micrometastatic epithelial cancer cells in bone marrow. J Clin Oncol 15(7):2701–2708

12. Pantel K, Izbicki JR, Angstwurm M, Braun S, Passlick B, Karg O, Thetter O, Riethmüller G (1993) Immunocytological detection of bone marrow micrometastasis in operable non-small cell lung cancer. Cancer Res 53(5):1027–1031
13. Silveira L Jr, Betiol Filho JA, Silveira FL, Zângaro RA, Pacheco MT (2008) Laser-induced fluorescence at 488 nm excitation for detecting benign and malignant lesions in stomach mucosa. J Fluoresc 18(1):35–40
14. Ducháč V, Zavadil J, Vránová J, Jirásek T, Stukavec J, Horák L (2011) Preoperative optical autofluorescence biopsy—verification of its diagnostic potential. Lasers Med Sci 26(3):325–333
15. Al-Salhi M, Masilamani V, Vijmasi T, Al-Nachawati H, Vijayaraghavan AP (2011) Lung cancer detection by native fluorescence spectra of body fluids—a preliminary study. J Fluoresc 21(2):637–645
16. Benmansour B, Stephan L, Cabon JY, Deschamps L, Giamarchi P (2010) Spectroscopic properties and laser induced fluorescence determination of some endocrine disrupting compounds. J Fluoresc 20(1):1–8
17. Lakowicz JR (1999) Principles of fluorescence spectroscopy, 2nd edn. Kluwer/Plenum, New York
18. Ramanujam N (2000) Fluorescence spectroscopy of neoplastic and non-neoplastic tissues. Neoplasia 2(1. 2):89–117
19. Chia TC, Sheng Fu, Yee Hong C, Leong Chuan K, Choong Leong Chia T, Sheng Fu, Yee Hong C, Kwek LC, Tang CL (2005) Application of laser-induced autofluorescence spectra detection system in human colorectal cancer in-vivo screening. Proc SPIE 5969:332–342
20. Chidananda SM, Satyamoorthy K, Rai L, Manjunath AP, Kartha VB (2006) Optical diagnosis of cervical cancer by fluorescence spectroscopy technique. Int J Cancer 119:139–145
21. Vladimirov B, Borisova E, Avramov L (2007) Delta-ALA-mediated fluorescence spectroscopy of gastrointestinal tumors: comparison of in vivo and in vitro results. Proc SPIE 6727:67271X
22. Wang CY, Chiang HK, Chen CT, Chiang CP, Kuo YS, Chow SN (1999) Diagnosis of oral cancer by light-induced autofluorescence spectroscopy using double excitation wavelengths. Oral Oncol 35 (2):144–150
23. Alfano RR, Tang GC, Pradhan A, Lam W, Choy DSJ, Opher E (1987) Fluorescence spectra from cancerous and normal human breast and lung tissues. IEEE J Quantum Electron 23:1806–1811
24. Hung J, Lam S, LeRiche JC, Palcic B (1991) Autofluorescence of normal and malignant bronchial tissue. Lasers Surg Med 11:99–105
25. Romer TJ, Fitzmaurice M, Cothren RM, Richards-Kortum R, Petras R, Sivak MV, Kramer LR, Romer TJ (1995) Laser-induced fluorescence microscopy of normal colon and dysplasia in colonic adenomas: implication for spectroscopic diagnosis. Am J Gastroenterol 90(1):81–87
26. Bottiroli G, Corce AC, Locatelli D, Marchesini R, Pignoli E, Tomatis S, Cuzzoni C, Palma SD, Dalfante M, Spinelli P (1995) Natural fluorescence of normal and neoplastic human colon: a comprehensive 'ex vivo' study. Lasers Surg Med 16:48–60
27. Ramanujam N, Mitchell MF, Mahadevan A, Thomsen S, Silva E, Richards-Kortum RR (1994) Fluorescence spectroscopy: a diagnostic tool for cervical intraepithelial neoplasia (CIN). Gynecol Oncol 52:31–38
28. Vo-Dinh T, Panjehpour M, Overholt BF (1998) Laser-induced fluorescence for esophageal cancer and dysplasia diagnosis. Ann N Y Acad Sci 838:116–122
29. Schantz SP, Kolli V, Savage HE, Yu G, Shah JP, Harris DE, Katz A, Alfano RR, Huvos AG (1998) In vivo native cellular fluorescence and histological characteristics of head and neck cancer. Clin Cancer Res 4(5):1177–1182
30. Thomas SS, Jayanthi JL, Subhash N, Thomas J, Mallia RJ, Aparna GN (2011) Characterization of dental caries by LIF spectroscopy with 404 nm excitation. Lasers Med Sci 26:299–305
31. Schantz SP, Savage HE, Sacks P, Alfano RR (1997) Native cellular fluorescence and its application to cancer prevention. Environ Health Perspect 4:941–944
32. Colasanti A, Kisslinger A, Fabbrocini G, Liuzzi R, Quarto M, Riccio P, Roberti G, Villani F (2000) MS-2 fibrosarcoma characterization by laser induced autofluorescence. Lasers Surg Med 26(5):441–448
33. Haringsma J, Tytgat GN (1999) Fluorescence and autofluorescence. Baillieres Best Pract Res Clin Gastroenterol 13(1):1–10
34. Thompson RC, Black KL, Kateb B, Marcu L (2002) Detection of experimental brain tumors using time-resolved laser-induced fluorescence spectroscopy. Proc SPIE 4613:8–12
35. Kim CK, Kalluru RR, Willard ST, Musselwhite AN, Yueh FY, Singh JP (2005) Optimized optical fiber laser-induced fluorescence (LIF) sensor for human breast cancer cell lines diagnosis. Proc SPIE 5993:60–65
36. Anidjar M, Cussenot O, Avrillier S, Ettori D, Teillac P, Le Duc A (1998) The role of laser-induced autofluorescence spectroscopy in bladder tumor detection. Dependence on the excitation wavelength. Ann N Y Acad Sci 838:130–142
37. Benson RC, Meyer RA, Zaruba ME, McKhann GM (1979) Cellular autofluorescence—is it due to flavins? J Histochem Cytochem 27(1):44–48
38. Demasa JN, Crosby GA (1971) The measurement of photoluminescence quantum yields.1 A review. Phys Chem 75(8):991–1024
39. Pesce AJ, Rosen C-G, Pasby TL (1996) Fluorescence spectroscopy: an introduction for biology and medicine. Publisher Books on Demand
40. Palmer GM, Keely PJ, Breslin TM, Ramanujam N (2003) Autofluorescence spectroscopy of normal and malignant human breast cell lines. Photochem Photobiol 78(5):462–469
41. Anidjar M, Cussenot O, Blais J, Bourdon O, Avrillier S, Ettori D, Villette JM, Fiet J, Teillac P, Le Duc A (1996) Argon laser induced autofluorescence may distinguish between normal and tumor human urothelial cells: a microspectrofluorimetric study. J Urol 155(5):1771–1774
42. Drezek R, Sokolov K, Utzinger U, Boiko I, Malpica A, Follen M, Richards-Kortum R (2001) Understanding the contributions of NADH and collagen to cervical tissue fluorescence spectra: modeling measurements and implications. J Biomed Opt 6 (4):385–396
43. Yicong Wu, Zheng W, Qu JY (2007) Detection of cell metabolism via wavelength and time-resolved intracellular autofluorescence. Proc SPIE 6430:64300A
44. Koenig F, McGovern FJ, Althausen AF, Deutsch TF, Schomacker KT (1996) Laser induced autofluorescence diagnosis of bladder cancer. J Urol 156(5):1597–1601
45. Na R, Stender IM, Wulf HC (2001) Can autofluorescence demarcate basal cell carcinoma from normal skin? A comparison with protoporphyrin IX fluorescence. Acta Derm Venereol 81(4):246–249
46. Grossman N, Ilovitz E, Chaims O, Salman A, Jagannathan R, Mark S, Cohen B, Mordechai S (2001) Fluorescence spectroscopy for detection of malignancy: H-ras overexpressing fibroblasts as a model. J Biochem Biophys Methods 50(1):53–63
47. Smith SR, Foster KR, Wolf GL (1986) Dielectric properties of VX-2 carcinoma versus normal liver tissue. IEEE Trans Biomed Eng 33(5):522–524
48. Bieling P, Rehan N, Winkler P, Helmke K, Maas R, Fuchs N, Bielack S, Heise U, Jurgens H, Treuner J, Romanowski R, Exner U, Kotz R, Winkler K (1996) Tumor size and prognosis in aggressively treated osteosarcoma. J Clin Oncol 14(3):848–858
49. Alfano RR, Das BB, Cleary J, Prudente R, Celmer EJ (1991) Light sheds light on cancer—distinguishing malignant tumors from benign tissues and tumors. Bull N Y Acad Med 67(2):143–150
50. Heintzelman DL, Utzinger U, Fuchs H, Zuluaga A, Gossage K, Gillenwater AM, Jacob R, Kemp B, Richards-Kortum RR (2000) Oral neoplasia using optimal excitation wavelengths for in vivo

detection of oral neoplasia using fluorescence spectroscopy. Photochem Photobiol 72(1):103–113
51. Mayinger B, Jordan M, Horbach T, Horner P, Gerlach C, Mueller S, Hohenberger W, Hahn EG (2004) Evaluation of in vivo endoscopic autofluorescence spectroscopy in gastric cancer. Gastrointest Endosc 59(2):191–198
52. Mayinger B, Jordan M, Horner P, Gerlach C, Muehldorfer S, Bittorf BR, Matzel KE, Hohenberger W, Hahn EG, Guenther K (2003) Endoscopic light-induced autofluorescence spectroscopy for the diagnosis of colorectal cancer and adenoma. J Photochem Photobiol B 70(1):13–20
53. Troyanova P, Borisova E, Avramov L (2007) Fluorescence and reflectance properties of hemoglobin-pigmented skin disorders. Proc SPIE 6734:673415
54. Hage R, Galhanone PR, Zângaro RA, Rodrigues KC, Pacheco MT, Martin AA, Netto MM, Soares FA, da Cunha IW (2003) Using the laser-induced fluorescence spectroscopy in the differentiation between normal and neoplastic human breast tissue. Lasers Med Sci 18(3):171–176
55. Chen W, He B, Wei GH, Gao G, Li S (1996) Laser-induced fluorescence spectroscopy of human normal and cancerous tissues. Proc SPIE 2887:156